Glass transition in a fluidized bed of hard spheres

Daniel I. Goldman* and Harry L. Swinney
Center for Nonlinear Dynamics and Department of Physics, The University of Texas at Austin, Austin, TX 78712
(Dated: November 14, 2005)

We demonstrate that a fluidized bed of hard spheres undergoes a glass transition during defluidization. As in other glass-forming systems, the dynamics of the bed becomes heterogeneous as the transition is approached; spatial and temporal correlation scales increase rapidly. Microscopic motion persists in the glass state, but the bed can be jammed (all motion arrested) by application of a small increase in flow rate. Thus a fluidized bed can serve as a test system for studies of the glass transition and jamming in hard sphere systems.

PACS numbers: 64.70.Pf,81.05.Rm,47.55.Kf,45.70.-n

Despite a century of study, there is no unified theory for the formation of a glass state from a liquid cooled below its freezing point (supercooled) [1, 2]. However, some signatures of the glass transition have been identified. One is the dependence of the volume of the glass on the cooling rate: the slower a liquid is cooled, the greater density it achieves when it forms a glass. Another signature is a rapid increase in a characteristic relaxation time (or viscosity) of the liquid during cooling as the glass transition temperature T_g is approached. In colloidal and hard sphere systems the transition is reached by increasing volume fraction ϕ rather than decreasing temperature; the transition occurs at $\phi_g \approx 0.58$ [3].

In liquids [4, 5, 6], colloids [3, 7, 8], simulations [9, 10, 11], and model systems [12, 13] it has been observed that as the glass transition is approached, the system dynamics becomes increasingly heterogeneous. Both the size of spatially correlated regions [14] and the time scale for rearrangement of these regions increase rapidly [7].

We examine a fluidized bed [15, 16], which is a vertical column of particles with a upward flow of fluid that maintains the particles in motion. We find that as the fluid flow rate Q is decreased, the system exhibits signatures of the glass transition. Two different volume fractions are found to characterize the behavior: $\phi_g \approx 0.585 \pm 0.003$, corresponding to the glass transition, and a larger volume fraction, $\phi_a \approx 0.594 \pm 0.004$, where ϕ becomes nearly independent of Q and only small scale motion persists; this motion can be stopped by a slight increase in flow rate, jamming the system. Our observed ϕ_a is close to the value where the system has the maximal number of statistically independent regions [17]; our ϕ_a is also close to the value obtained for slow defluidization of particles in a gas fluidized bed [18].

Experiment — Water flows upward at a volume flow rate Q through a vertical column of glass spheres in a square bore glass tube of cross sectional area $A = 5.81$ cm^2. There are 4×10^6 glass spheres with diameter $d = 250 \pm 8$ μm and density $\rho_p = 2.47$ g/cm^3. Fluid flow rate fluctuations are smaller than 0.3%. To obtain a uniform flow, fluid passes into the bottom of the column through a nylon mesh (5 μm weave, open area 0.75%, Nitex mesh, Sefar America). The average height h of the bed top surface above the distributor is measured to determine the average bed solid volume fraction, $\phi = M_p/\rho_p A h$, where M_p is the total mass of the particles. We measure the fluid pressure drop ΔP from the bottom to the top of the bed; the values will be given normalized by the buoyant weight of the grains. The dynamics of the bed are studied by imaging of the side of the bed and by using the light scattering method called Diffusing Wave Spectroscopy (DWS) [19] to probe the interior of the bed.

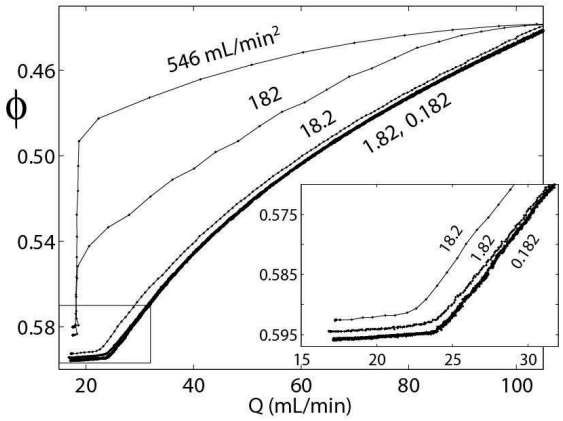

FIG. 1: The volume fraction achieved during defluidization depends on the rate at which the flow is reduced, just as in the glass transition in colloids and in hard sphere models. The number next to each curve indicates the ramp rate as fluid flow rate Q is decreased through the defluidization transition ($Q \approx 24$ mL/min). In the top two curves the ramping is so rapid that the final state is achieved through sedimentation. Inset: magnification of the region near the arrest transition at $\phi_a = 0.594$.

Signatures of the glass transition— The dependence of ϕ on the ramping rate (Fig. 1) is similar to the dependence of glass volume on cooling rate in supercooled liquids that form glasses [1]. In the fluidized bed for suf-

ficiently large Q, the grains are mobile [20] and $\Delta P \cong 1$. However, as Q decreases, particle mobility decreases and ϕ increases until the defluidization transition is reached at ϕ_a (the knee of the curve in the inset of Fig. 1); ϕ_a decreases only 1% as the "cooling rate" dQ/dt is decreased by three orders of magnitude.

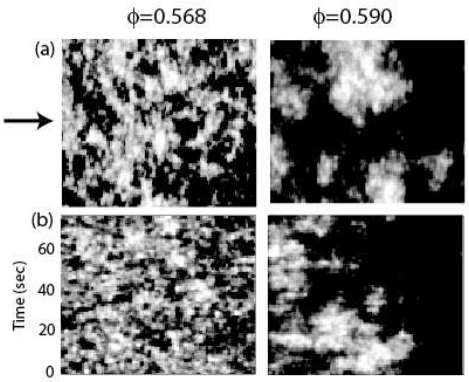

FIG. 2: Dynamical heterogeneity: as the glass state is approached, immobile regions (black) and mobile regions (white) grow in size, as shown in the images in (a). Each panel in (a) is the difference between two images (1.5×1.5 cm^2) of the side of the bed taken 0.3 s apart; the difference images have been thresholded and scaled to aid visualization. The lifetime of immobile regions also increases as the transition is approached, as illustrated by the raster scan in (b), which shows the time evolution of a single row of pixels (indicated by arrow) from (a). The flow rates for $\phi = 0.568$ and $\phi = 0.590$ were respectively 26.19 and 33.02 mL/min. In this figure and in Fig. 3, the data were obtained at ϕ values reached by decreasing Q at the slowest ramp rate in Fig. 1.

Additional signatures of a glass transition in the fluidized bed are dynamical heterogeneity, illustrated in Fig. 2, and changes in various bed properties, shown in Fig. 3. As in other glass-forming systems [4, 7, 9, 13], the fluidized bed mobility becomes heterogeneous and the size of the mobile regions increases as ϕ increases, as illustrated by the images in Fig. 2(a) and by the correlation range ξ plotted in Fig. 3(a). (ξ is given by the $1/e$ point of azimuthal average of 2D autocorrelation of difference images.) The decrease in ξ beyond ϕ_g is similar to the decrease in length scale of cooperative regions observed in colloid experiments [7] and lattice model simulations [22]. The observed decrease in ξ likely arises because the dynamics has slowed enough at ϕ_g so that no discernible motion occurs during the measurement (0.3 s). At ϕ_g we also observed a change in $d(\Delta P)/dQ$, as shown in Fig. 3(d); we conjecture that this increase at ϕ_g is a consequence of the sidewall support of the transiently immobile regions. We also made movies of the top surface of the bed, and these too exhibited dynamical heterogeneities – volcanos and channels, as observed in studies of gas fluidized beds [23, 24, 25, 26].

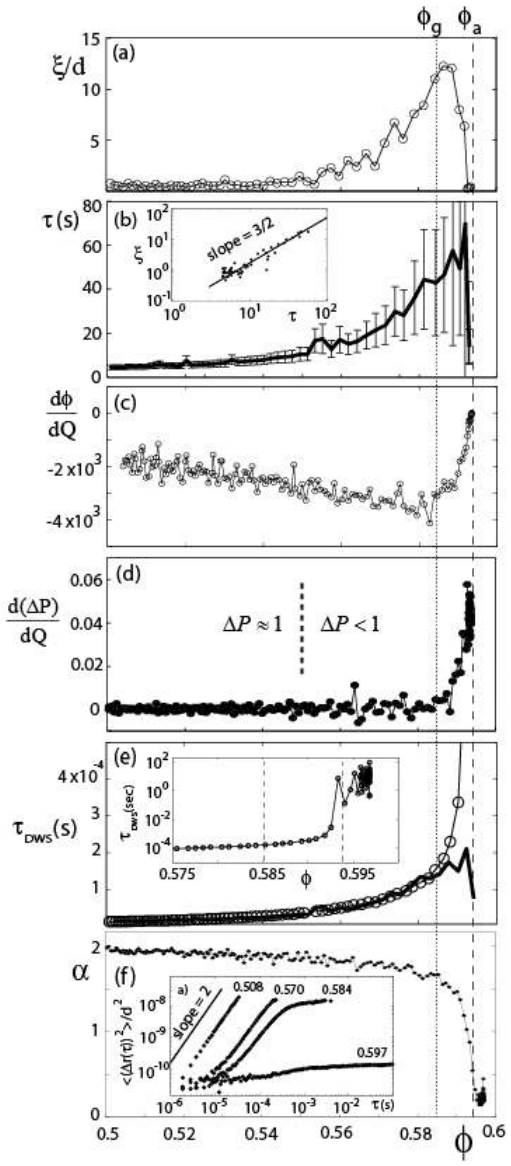

FIG. 3: Measurements on a fluidized bed reveal two transitions: a hard sphere glass transition at $\phi_g \approx 0.585$ [21] and an arrest transition at $\phi_a \approx 0.594$. (a) An increase near ϕ_g in the spatial correlation length ξ of mobile regions (Fig. 2(a)), and a decrease in ξ beyond ϕ_g to $\xi = 0$ at ϕ_a. (b) An increase in the average correlation time in bed images (Fig 2(b)). The inset shows a power law dependence of ξ on τ near ϕ_g. (c) An inflection in $d\phi/dQ$ at ϕ_g and a divergence in $d\phi/dQ$ as ϕ_a is approached. (d) An increase in $d(\Delta P)/dQ$ beyond ϕ_g and a peak at ϕ_a, where $d(\Delta P)/dQ$ becomes independent of Q. (e) An increase in the decorrelation time $\tau_{\rm DWS}$ of the intensity autocorrelation function of transmitted laser light [19] near ϕ_g. The bold solid curve, the correlation time from (d) scaled by 3×10^5, begins to deviate from $\tau_{\rm DWS}$ at ϕ_g. Inset: at the arrest transition $\tau_{\rm DWS}$ no longer increases. (f) A decrease in the exponent α for the Mean Square Displacement (MSD) (for intermediate times) near ϕ_g. Inset: time dependence of MSD.

The lifetime τ of mobile and immobile regions increases as ϕ increases, as illustrated by the space-time plots in Fig. 2(b) and by the correlation time τ plotted in Fig. 3(b). (τ is the $1/e$ point of the time autocorrelation function.) The standard deviation of the distribution of decay times (denoted by vertical bars in Fig. 3(b)) also increases as ϕ increases, just as in a hard sphere model [22]. The increase in time scales with increasing ϕ is similar to that found in experiments [6] and simulations on colloidal systems and polymers [9] and hard sphere models [13]. The length and time scales for $\phi < \phi_g$ are linked by a power law, as shown in the inset of Fig. 3(b). A power law was also obtained in a study of a lattice model [22], but with an exponent value $1/4$ rather than the $3/2$ given by our observations.

The bulk properties of the bed also change markedly at ϕ_g: $d\phi/dQ$ reaches a minimum (Fig. 3(a)), and the pressure drop across the bed ΔP begins to rapidly decrease, dropping well below the weight of the bed [27]. Further, $d(\Delta P)/dQ$ begins to increase rapidly at ϕ_g until the increase is arrested at ϕ_a (Fig. 3(b)), beyond which the bed has defluidized and ΔP becomes linear with Q, following Darcy's law.

Additional evidence of the glass transition is provided by information on bed behavior on short time scales. Measurements of the intensity-intensity correlation function $g^{(2)}(\tau)$ of light multiply scattered as it travels through through the bed [28] provide the time scale $\tau_{\rm DWS}$ (the $1/e$ point on the curve), shown in Fig. 3(e). $\tau_{\rm DWS}$ increases with the *same* functional form as the decorrelation time of image pixel intensity τ (see Fig. 3(d)), until ϕ_g. The correspondence in the behavior for times differing by a factor of $\sim 10^4$ indicates that, as in other glass systems [1], the macro and microscopic degrees of freedom are equivalent prior to the glass transition and become decoupled after it occurs.

Information on bed behavior at small length scales was obtained using Diffusing Wave Spectroscopy (DWS) theory [19] to invert the autocorrelation curves and obtain $\langle \Delta r(t)^2 \rangle$, the mean square displacement (MSD) of the grains at times so short that particles moved only $\sim 0.01\%$ of their diameter. For $\phi \ll \phi_g$, the short time dynamics is well described by $\langle \Delta r(t)^2 \rangle \propto \tau^\alpha$ with $\alpha \approx 2$ (see inset of Fig. 3(f)), indicating that all grains undergo ballistic motion between collisions [20, 29]. For $\phi \gtrsim 0.54$, as ϕ approaches ϕ_g, the curves develop a region with $\alpha < 2$ at short times, indicating that at these times the particles remain in contact with neighbors. However, at larger times, $\alpha \approx 2$, as can be seen in the inset of Fig. 3(f), indicating that the particles move ballistically. As ϕ approaches ϕ_g, the MSD develops a plateau region at longer times, indicating the particles are caged; caging has been observed in hard sphere systems that approach the glass state [7, 10]. For $\phi > \phi_g$, the slope at intermediate times decreases, indicating that particles are no longer able to break from their cages, and α rapidly decreases (Fig. 3(f)). For $\phi > \phi_a$, all particles are immobile on macroscopic length scales (Fig 3(a), (b) and (e)).

Jamming — Even in the arrested state, microscopic motion persists – this is shown in Fig. 4(b) for a line of light (multiply scattered by the bed) imaged on a CCD camera with 30 ms exposure such that each pixel views a single coherence area [30]. The intensity of each pixel fluctuates, even for $\phi > \phi_a$, indicating that microscopic motion persists. However, all microscopic motion can be jammed (stopped) by slightly increasing Q (for any $\phi > \phi_g$); the DWS could detect motion of only 1 nm for any scattering particle. The jamming presumably establishes the stress backbone of the system [31] and explains the hysteresis seen in Fig. 4(c). Once the system is jammed, increases and decreases in Q below the onset of fluidization [15] do not change ϕ. Such jamming has been associated with glass states [31, 32, 33] and has been studied in fluidized beds [34].

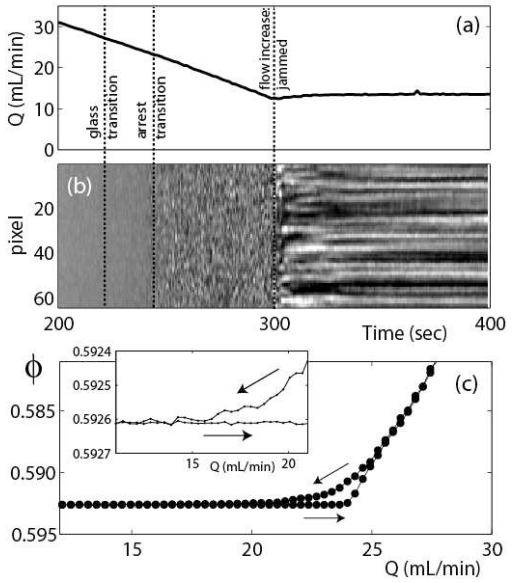

FIG. 4: Microscopic motion in the glass state is halted by a slight increase in Q, jamming the system. (a) Q is decreased at 9.6 mL/min^2 until it reaches $Q \approx 12.5$ mL/min, at which point it is increased by 1 mL/min (indicated by the rightmost dashed line). The glass state (when $\Delta P < 1$) is achieved at $Q = 24$ mL/min, indicated by the leftmost dashed line. (b) The speckle field corresponding to the flow in (a) becomes time independent after jamming occurs. (c) The hysteresis in ϕ for increasing and increasing Q after an increase in Q at $Q \approx 8$ mL/min. The hysteresis disappears for $\phi > \phi_g$. The flow ramp protocol is described in [21]. Inset: detail of hysteresis.

Discussion—The fluidized bed system exhibits the essential features of a glass transition: rate dependence on final state, dynamical heterogeneity, rapid increase in time scale, and jamming. Once the bed forms a glass at ϕ_g, it is unable to continue to pack sufficiently (increase

ϕ) in response to changes in Q, as it would in the fluidized states. Thus the glass transition triggers the final arrest of the bed—defluidization is a consequence of the glass transition. Since ϕ_g is a property of hard spheres, this explains the slightly larger arrest volume fraction ϕ_a seen in our fluidized bed and that of Menon and Durian [20]; ϕ_a is independent of particle size, density, and aspect ratio (see [18]). We speculate that the Random Loose Packed volume fraction, $\phi_{\mathrm{RLP}} \approx 0.56$, plays a role in the onset of heterogeneity. The volume fraction transition values depend weakly on surface properties [17] and strongly on cohesive effects [27].

Since a fluidized bed is a simple system that allows fine control, it an ideal system for studying glass and jamming transitions and for informing theory [35]. Further, understanding glass behavior in a fluidized bed can inform fluidized bed design, which is important in many industrial applications [15].

We thank Mark Shattuck for experimental assistance and discussion, and Matthias Schröter, David Chandler, Albert Pan, Juan Garrahan and Eric Weeks for helpful discussions. This work was supported by Robert A. Welch Foundation and the Office of Basic Energy Sciences of the U.S. Department of Energy.

* digoldma@berkeley.edu; URL: http://socrates.berkeley.edu/~digoldma; Present address: Department of Integrative Biology, The University of California at Berkeley, Berkeley, CA 94720-3140

[1] M. D. Ediger, C. A. Angell, and S. R. Nagel, J. Phys. Chem. **100**, 13200 (1996).
[2] P. G. Debenedetti and F. H. Stillinger, Nature **410**, 259 (2001).
[3] P. N. Pusey and W. V. Megan, Phys. Rev. Lett. **59**, 2083 (1987).
[4] M. D. Ediger, Annu. Rev. Phys. Chem. **51**, 99 (2000).
[5] U. Tracht, M. Wilhelm, A. Heuer, K. Schmidt-Rohr, and H. W. Spiess, Phys. Rev. Lett. **81**, 2727 (1998).
[6] X. Qiu and M. D. Ediger, J. Chem. Phys. B **107**, 459 (2003).
[7] E. R. Weeks, J. C. Crocker, A. C. Levitt, A. Schofield, and D. A. Weitz, Science **287**, 627 (2000).
[8] W. van Megan and S. M. Underwood, Phys. Rev. E **49**, 4206 (1994).
[9] S. C. Glotzer, J. Non-Cryst. Solids **274**, 342 (2000).
[10] B. Doliwa and A. Heuer, Phys. Rev. Lett. **80**, 4915 (1998).
[11] R. J. Speedy, Mol. Phys. **95**, 169 (1998).
[12] E. Bertin, J.-P. Bouchaud, and F. Lequeux, cond-mat/0501192 (2005).
[13] J. P. Garrahan and D. Chandler, Phys. Rev. Lett **89**, 035704 (2002).
[14] G. Adam and J. H. Gibbs, J. Chem. Phys. **43**, 139 (1965).
[15] R. Jackson, *The Dynamics of Fluidized Particles* (Cambridge University Press, 2000).
[16] S. Sundaresan, Annu. Rev. Fluid Mech. **35**, 63 (2003).
[17] M. Schröter, D. I. Goldman, and H. L. Swinney, Phys. Rev. E **71**, 030301 (2005).
[18] R. Ojha, N. Menon, and D. J. Durian, Phys. Rev. E **62**, 4442 (2000).
[19] D. A. Weitz and D. J. Pine, in *Dynamic Light Scattering: The method and some applications*, edited by W. Brown (Clarendon Press, 1993), pp. 653–720.
[20] N. Menon and D. J. Durian, Phys. Rev. Lett. **79**, 3407 (1997).
[21] Each curve was obtained over a period of 100 s after waiting for 30 s after the target flow rate had been achieved. The target flow rate was approached at $0.58\mathrm{mL/min}^2$, close to the lowest ramp rate in Fig. 1.
[22] A. C. Pan, J. P. Garrahan, and D. Chandler, cond-mat/0410525 (2004).
[23] P. Duru, M. Nicolas, J. Hinch, and E. Guazzelli, J. Fluid Mech. **452**, 371 (2002).
[24] L. Massimilla, G. Donsi, and C. Zucchini, Chem. Eng. Sci. **27**, 2005 (1972).
[25] S. C. Tsinontides and R. Jackson, J. Fluid Mech. **255**, 237 (1993).
[26] J. M. Valverde, M. A. S. Quintanilla, A. Castellanos, and P. Mills, Phys. Rev. E **67**, 016303 (2003).
[27] J. M. Valverde, A. Castellanos, and M. A. S. Quintanilla, Phys. Rev. Lett. **86**, 3020 (2001).
[28] We determine l^*, the scattering length over which photon orientation is uncorrelated, by using a high speed camera (Phantom 4, Vision Research) to estimate the collision velocity of particles near the side of the bed at a known Q. We then compute l^* for each volume fraction by taking the ratio of volume fractions. We find that for all volume fractions $L/l^* \gtrapprox 10$.
[29] N. Menon and D. J. Durian, Science **275**, 1920 (1997).
[30] A. P. Y. Wong and P. Wiltzius, Rev. Sci. Instrum. **64**, 2547 (1993).
[31] C. S. O'Hern, S. A. Langer, A. J. Liu, and S. R. Nagel, Phys. Rev. Lett **86**, 111 (2001).
[32] A. J. Liu and S. R. Nagel, Nature **396**, 21 (1998).
[33] C. S. O'Hern, L. E. Silbert, A. J. Liu, and S. R. Nagel, Phys. Rev. E **68**, 011306 (2003).
[34] J. M. Valverde, M. A. S. Quintanilla, and A. Castellanos, Phys. Rev. Lett. **92**, 258303 (2004).
[35] M. Z. Bazant, cond-mat/0307379 (2004).